



## Article

# Electron Bombardment of Amorphous Thione Ices—Thioacetamide as a Case Study

Sándor Góbi<sup>1,\*</sup>, Barbara Keresztes<sup>1,2</sup> and György Tarczay<sup>1,3</sup><sup>1</sup> Laboratory of Molecular Spectroscopy, Institute of Chemistry, ELTE Eötvös Loránd University, H-1518 Budapest, Hungary<sup>2</sup> Hevesy György PhD School of Chemistry, Institute of Chemistry, ELTE Eötvös Loránd University, H-1518 Budapest, Hungary<sup>3</sup> Centre for Astrophysics and Space Science, ELTE Eötvös Loránd University, H-1518 Budapest, Hungary

\* Correspondence: sandor.gobi@ttk.elte.hu

**How To Cite:** Góbi, S.; Keresztes, B.; Tarczay, G. Electron Bombardment of Amorphous Thione Ices—Thioacetamide as a Case Study. *Photochemistry and Spectroscopy* 2025, 1(1), 3. <https://doi.org/10.53941/ps.2025.100003>

Received: 3 October 2025

Revised: 7 November 2025

Accepted: 12 November 2025

Published: 19 November 2025

**Abstract:** Amorphous thioacetamide (TA) ice was deposited at 10 K and was bombarded with 5 keV electrons. TA ices were shown to decompose into acetonitrile (ACN,  $\text{H}_3\text{C}-\text{C}\equiv\text{N}$ ), cyanide anion ( $[\text{CN}]^-$ ), and ketenimine ( $\text{H}_2\text{C}=\text{C}=\text{NH}$ ). The experiments were repeated with TA ices mixed with  $\text{H}_2\text{O}$ , to assess the effect of an oxygen source. In this case, the formation of cyanate anion ( $[\text{OCN}]^-$ ) was also observed besides those seen in the pure TA ice experiment. This study is the first that aims to reveal the decomposition pathways of a thioamide upon energetic irradiation in the low-temperature ice phase.

**Keywords:** thioacetamide; amorphous ice; electron irradiation; infrared spectroscopy

## 1. Introduction

The decomposition of sulfurous compounds has long been studied to answer questions arising in various scientific fields, such as sulfur depletion in astrochemistry [1]. Among the numerous applicable radiation sources, electron irradiation is a widely used technique, which aims to mimic the secondary electrons forming in the wake of galactic cosmic ray particles [2,3]. A pioneering work was done by Carlson et al. who exposed elemental sulfur dispersed in  $\text{H}_2\text{O}$  to energetic electrons, pointing out the possibility of sulfuric acid ( $\text{H}_2\text{SO}_4$ ) formation on the Jovian moon Europa [4]. Later, Maity & Kaiser performed the electron bombardment of pure carbon disulfide ( $\text{CS}_2$ ) and its mixture with molecular oxygen ( $\text{O}_2$ ), proving the formation of higher-order carbon sulfides ( $(\text{CS})_x$ , where  $x = 4-6$ ) or sulfur oxides such as sulfur dioxide ( $\text{SO}_2$ ) and sulfur trioxide ( $\text{SO}_3$ ) along with carbonyl sulfide (OCS) [5,6]. These studies suggested that  $\text{CS}_2$  can be easily converted into OCS by reacting with suprathreshold O atoms, which latter can be formed from various oxygen sources like  $\text{H}_2\text{O}$ , carbon dioxide ( $\text{CO}_2$ ), or methanol ( $\text{CH}_3\text{OH}$ ) when exposed to ionizing radiation. Sivaraman studied the  $\text{CO}_2:\text{CS}_2$  ice mixture analogous to those found on the surface of icy satellites and interstellar icy mantles and observed the formation of OCS,  $\text{SO}_2$ , ozone ( $\text{O}_3$ ), carbon trioxide ( $\text{CO}_3$ ),  $\text{SO}_3$ , carbon subsulfide ( $\text{C}_3\text{S}_2$ ), and carbon monoxide (CO) upon bombarding the sample with electrons in the keV energy range [7]. A more complex, quaternary ice mixture was investigated by Mahjoub and coworkers; they processed  $\text{H}_2\text{O}:\text{ammonia} (\text{NH}_3):\text{CH}_3\text{OH}:\text{hydrogen sulfide} (\text{H}_2\text{S})$ , modeling Jupiter Trojan ices [8]. During the temperature-programmed desorption (TPD) phase of the experiments, sublimation of small sulfur allotropes ( $\text{S}_3$  and  $\text{S}_4$ ) was recorded. The authors hypothesized that these metastable molecules may polymerize into the stable  $\text{S}_8$  form, which may affect the spectral reflectance of Jupiter Trojans. The formation of organosulfur compounds was also reported along with the sulfur allotropes. Mifsud et al. examined the electron-induced decay of  $\text{H}_2\text{S}$  and  $\text{SO}_2$ , both in amorphous and crystalline states [9]. The formation of dihydrogen disulfide ( $\text{H}_2\text{S}_2$ ) was observed in the case of  $\text{H}_2\text{S}$ , whereas the main product was  $\text{SO}_3$  in the irradiated  $\text{SO}_2$  samples. On one hand, they found proof for phase-dependent chemistry; amorphous  $\text{H}_2\text{S}$  seems to be more sensitive to irradiation than its crystalline counterpart. On the other hand, the radiation kinetics of  $\text{SO}_2$  exhibits dependence on the



**Copyright:** © 2025 by the authors. This is an open access article under the terms and conditions of the Creative Commons Attribution (CC BY) license (<https://creativecommons.org/licenses/by/4.0/>).

**Publisher's Note:** Scilight stays neutral with regard to jurisdictional claims in published maps and institutional affiliations.

fluences; the crystalline sample appears to be more susceptible to the low-fluence regime. In contrast, both phases undergo slow decays in the high-fluence regime. The authors also made an attempt to rationalize their findings and the formation of sulfur allotropes in the context of interstellar and Solar System ice astrochemistry. Later, the irradiation chemistry of the H<sub>2</sub>S:CO system was in the focus of interest, which yielded thioformic acid (HC(=O)SH) as the main product [10]. Recently, Martín-Doménech et al. unraveled the formation mechanism of OCS by irradiating CO<sub>2</sub>:CS<sub>2</sub> ice mixtures [11]. Two formation pathways were considered: sulfurization of CO and oxidation of the CS intermediate; the latter was preferred based on the experimental results in line with earlier theoretical predictions. The authors also assessed the influence of O sources other than CO, such as CO<sub>2</sub> and H<sub>2</sub>O and detected numerous S-containing molecules besides OCS, e.g., SO<sub>2</sub>, C<sub>3</sub>S<sub>2</sub>, and S<sub>2</sub>.

Thioamides, molecules with a –C(=S)–NH– domain, represent a step forward in understanding the radiation chemistry of sulfur-containing compounds, and they have been studied several times under vastly different circumstances (e.g., [12,13]). Among them, thioacetamide (TA, H<sub>3</sub>C–C(=S)–NH<sub>2</sub>) has garnered a particular interest by the present authors in the past several years. The investigations were carried out both in the amorphous ice phase as well as in cryogenic matrices, in which the samples were exposed to a wide variety of radiation sources such as broadband and laser UV photons or H atoms [14–17]. The decomposition mechanism of TA, however, has not been examined in the low-temperature amorphous ice phase so far. The present work addresses to fill in this gap, further extending our knowledge on the radiation chemistry of sulfurous compounds. This work also aims to unravel the influence of H<sub>2</sub>O as an oxygen source on the TA decomposition.

## 2. Experimental

The experiments were performed on the VIZSLA setup, which contains an ultrahigh-vacuum (UHV) compatible stainless steel simulation chamber that can be pumped down to a base pressure of  $\approx 10^{-9}$  mbar when cooled [18]. The amorphous TA (Sigma-Aldrich (St. Louis, MI, USA), > 99%) ice was prepared on a gold-plated silver wafer of  $\approx 1$  cm<sup>2</sup> (referred to as substrate hereafter), which was cooled down to 10.0 K by the RDK-415D cryostat of the setup (Sumitomo Heavy Industries Inc. (Tokyo, Japan)). The TA sample had been inserted in a small glass vial before the experiment; the sample container is directly attached to the experimental setup, separated by a valve. The sample inlet continued inside the vacuum chamber as a Teflon tube 6 mm in outer diameter ending approximately 3 cm before the substrate. The TA sample was kept at room temperature, which ensured sufficient vapor pressure for the deposition. In the case of the experiments involving TA:H<sub>2</sub>O ices, distilled H<sub>2</sub>O was introduced via a leak valve and a stainless steel capillary array with its tip arranged ca. 3 cm from the substrate.

A Specs EQ 22 electron gun produced the high-energy electrons that bombarded the sample (electron kinetic energy was set to  $\approx 5$  keV, nominal emission current was set to 100 nA). Due to the limited penetration depth of the electrons, typically in the several hundred nm range, multiple deposition–irradiation cycles had to be done in order to let the decomposition products accumulate. Accordingly, a deposition cycle of 40 min was followed by 30 min of electron bombardment; these cycles were repeated four times in total. When preparing the TA:H<sub>2</sub>O ice mixture, four deposition–irradiation cycles were performed; the deposition and electron bombardment lasted 20 and 30 min, respectively. Then, the TPD study was carried out on the samples, using a heat ramp of 1 K min<sup>-1</sup> to the temperature of 300 K. Two parallel irradiation experiments were done to ensure the reproducibility of the results. Control (or blank) experiments using identically prepared samples but without irradiation were also carried out. Besides, one irradiation experiment was also done with neat H<sub>2</sub>O ice using the same deposition–irradiation conditions as in the TA:H<sub>2</sub>O experiment.

The mid-IR (MIR) spectra were collected by means of a Bruker Invenio FT-IR spectrometer with a liquid N<sub>2</sub>-cooled mid-band Mercury Cadmium Telluride (MCT) detector. The spectral collection occurred in reflection–absorption mode, in the region of 4000–600 cm<sup>-1</sup>, at a resolution of 0.5 cm<sup>-1</sup>, averaging 32 scans. A background spectra of 256 scans were taken right before the start of the sample deposition. Quantum-chemical Density Functional Theory (DFT) computations were performed using the Gaussian G09 software at the B3LYP/cc-pVTZ level of theory to assist the vibrational assignment of the acetonitrile (or methyl cyanide, H<sub>3</sub>C–C $\equiv$ N, ACN hereafter) band at 2290 cm<sup>-1</sup> [19]. After geometry optimization, anharmonic vibrational frequencies and intensities of the geometry possessing the minimum energy on the potential energy surface were computed. The anharmonic properties were obtained using the VPT2 method as implemented in the G09 software [20,21]. The obtained geometry as well as the vibrational frequencies and intensities are summarized in Tables S1 and S2 in the Supplementary Materials.

The thicknesses can be computed based on column density  $N$  in cm<sup>-2</sup>, Section 0) by applying the formula:

$$d = \frac{10^7 N}{\rho N_{\text{Av}}}$$

where  $d$  is the ice thickness (in nm),  $M$  denotes the molar mass of TA ( $75.13 \text{ g mol}^{-1}$ ),  $\rho$  signifies the ice density (crystalline,  $1.319 \text{ g cm}^{-3}$ ) [22], and  $N_{\text{Av}}$  indicates Avogadro's number. The thickness of the neat TA sample was determined to be  $49 \pm 4 \text{ nm}$ . It must be emphasized that since multiple deposition–irradiation cycles were conducted, the thickness of the sample in the control experiment was considered, even though a thickness in the same order of magnitude is expected for the sample in the one involving the electron irradiation at the end of the fourth deposition cycle. Furthermore, since there is no data on many properties of the amorphous TA ice, the thickness was calculated for the sample that was already crystallized, based on the spectra taken at 200 K. As far as the thickness and the mixing ratio of TA:H<sub>2</sub>O ice mixture are concerned, they were determined as  $63 \pm 9 \text{ nm}$  and  $1:5 \pm 1$ , respectively. The TA:H<sub>2</sub>O ratio was calculated from their respective  $N$  values. For the sample thickness, the weighted average values of the TA and H<sub>2</sub>O components were used ( $M[\text{H}_2\text{O}] = 18.02 \text{ g mol}^{-1}$ ,  $\rho[\text{H}_2\text{O}] = 0.93 \text{ g cm}^{-3}$ ) [23]. The used average values were  $M[\text{mix}] = 28 \pm 2 \text{ g mol}^{-1}$ ,  $\rho[\text{mix}] = 1.00 \pm 0.01 \text{ g cm}^{-3}$ . CASINO simulations were also performed to assess the dose the TA molecules absorbed during electron irradiation (Table S3 in the Supplementary Materials) [24].

### 3. Results

#### 3.1. Electron Bombardment of Neat TA Ice

The mid-infrared (MIR) spectrum of the freshly deposited amorphous TA ice is in good agreement with the one obtained previously on the same experimental setup (black trace of Figure 1a, the band maxima are listed in Table S4 in the Supplementary Materials) [17]. The assignment of the TA bands in the ice phase are provided by an even earlier study [14]. The appearance of new features can be observed upon exposing the sample to 5 keV electrons, the center of these broad bands are found at 2288, 2253, 2068, and 2029  $\text{cm}^{-1}$  (Figure 1a, red trace). Out of these four bands, three can be assigned based on earlier results. The first two bands are attributable to ACN [25,26], whereas the last one is caused by its isomer, ketenimine ( $\text{H}_2\text{C}=\text{C}=\text{NH}$ ) [27]. In contrast, revealing the carrier of the third band is less straightforward. According to studies focusing on similar systems, one could contemplate that this band belongs to the absorption of the cyanide anion ( $[\text{CN}]^-$ ) since its shape shares similarities with the ones presented by earlier works focusing on the formation of  $[\text{CN}]^-$  in irradiated cryogenic ices, although it is shifted towards lower wavenumbers compared to the literature value ( $2081 \text{ cm}^{-1}$ ) [27,28]. Alternatively, the formation of thiocyanate anion ( $[\text{SCN}]^-$ ) could also explain the presence of the  $2068 \text{ cm}^{-1}$  band although there is no ice-phase literature data on its IR absorptions; the gas-phase value is  $2066 \text{ cm}^{-1}$  [29]. A VUV photolytic / energetic electron bombardment study of the oxygen-bearing analog urea ( $\text{H}_2\text{N}-\text{C}(=\text{O})-\text{NH}_2$ ) even proposed the formation of  $\text{HNCO}/[\text{OCN}]^-$ , which could suggest  $\text{HNCS}/[\text{SCN}]^-$  as products in our case [30]. However, no traces of HNCS were detected in our irradiated sample. Moreover, the anionic forms exhibit a shift towards shorter wavenumbers with regard to their protonated counterparts both in the case of the  $\text{HCN}/\text{CN}^-$  ( $2107/2081 \text{ cm}^{-1}$ ,  $\Delta\tilde{\nu} = -36 \text{ cm}^{-1}$ ) and  $\text{HNCO}/\text{OCN}^-$  systems ( $2260/2165 \text{ cm}^{-1}$ ,  $\Delta\tilde{\nu} = -95 \text{ cm}^{-1}$ ) [27,30,31]. One may deduce from these findings that in the case of the  $\text{HNCS}/[\text{SCN}]^-$  system, the position of  $[\text{SCN}]^-$  is expected to be dozens of wavenumbers below that of HNCS ( $2057 \text{ cm}^{-1}$ ) [32]. In other words, the carrier of the  $2068 \text{ cm}^{-1}$  band cannot be the  $[\text{SCN}]^-$  anion. Table 1 summarizes the band assignments.

**Table 1.** Assignment of the bands appearing during electron irradiation of amorphous TA ice.

Wavenumber ( $\text{cm}^{-1}$ )	Literature Value	Molecule	Assignment <sup>a</sup>	Ref.
2288	2289	ACN	$\nu[\text{CC}] + \beta_s[\text{CH}_3]$ <sup>b</sup>	[25]
2253	2252	ACN	$\nu[\text{C}\equiv\text{N}]$	[25]
2068	2081	$[\text{CN}]^-$	$\nu[[\text{CN}]^-]$	[27,28]
2029	2033	$\text{H}_2\text{C}=\text{C}=\text{NH}$	$\nu_{\text{as}}[\text{C}=\text{C}=\text{NH}]$	[27]

<sup>a</sup>  $\nu$ : stretching;  $\beta$ : bending;  $s$ : symmetric;  $as$ : antisymmetric; <sup>b</sup> Combination band. Assignment made based on anharmonic computations at the B3LYP/cc-pVTZ level of theory using the Gaussian G09 software [19]; Fermi-resonance is predicted with the  $\nu[\text{C}\equiv\text{N}]$  mode.

In comparison, when TA samples dispersed in inert cryogenic matrices were exposed to energetic radiation, the formation of similar decay products could be observed [15]. ACN and its isomer,  $\text{H}_2\text{C}=\text{C}=\text{NH}$  were doubtlessly identified in the matrix after Lyman- $\alpha$  or laser UV irradiation with the mixing ratio (relative abundance in ppm) of the former being one of the highest among the irradiation products. Although  $[\text{CN}]^-$  could not be detected in the processed matrix-isolated samples, their protonated counterparts, hydrogen cyanide (HCN) and hydrogen isocyanide (HNC), were present, which is plausible considering the H-rich environment of the *para*-H<sub>2</sub> matrix.

Even thiols were formed, which is in contrast to the current study, where their extremely weak absorption bands cannot be observed. Note that the formation of thiols was also shown both in amorphous ice phase and in *para*-H<sub>2</sub> matrix when TA was exposed to H atoms [16,17]. The difference between the results obtained in amorphous ice and in cryogenic matrices can be substantiated by the fact that energetic electron irradiation was used in the present experiment, whereas UV irradiation was performed on the matrix-isolated samples. In general, electron irradiation can be considered less selective, more bonds can break than in the case of UV irradiation. Besides, in ice phase, more secondary reactions may take place than in a cryogenic matrix.

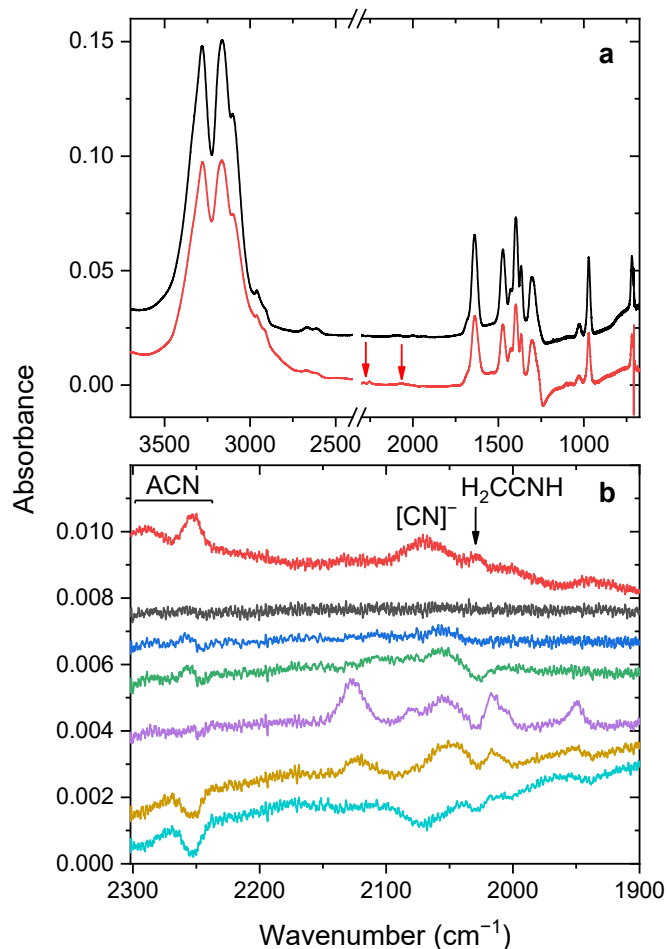


**Figure 1.** (a) MIR spectra (3600–675 cm<sup>-1</sup> region) of neat solid TA in the control (black trace) and electron bombardment (red trace) experiments. The red arrows show the newly forming bands. (b) MIR spectra (2300–1900 cm<sup>-1</sup> region) of neat solid TA in the beginning of the TPD phase (red trace). Difference spectra as obtained at 50 K (dark gray), 100 K (blue), 150 K (green), 200 K (purple), 250 K (dark yellow), and 300 K (turquoise), respectively; the spectra taken at the beginning of the TPD phase served as reference. The spectra are offset for clarity.

Figure 1b shows a section of the MIR spectra of the processed TA ice before the TPD phase as well as difference spectra when the sample is gradually warmed up. The full spectrum can be found in the Supplementary Materials (Figure S1). As can be seen, no spectral changes occur by the temperature of 50 K (Figure 1b, dark gray trace) but the band attributed to H<sub>2</sub>C=C=NH is already decreasing at 100 K, whereas those of the ACN molecule increase (Figure 1b, blue trace). This phenomenon is even more pronounced at 150 K (Figure 1b, green trace). The TA ice starts crystallizing above this temperature, which process is already finished by 200 K; this manifests itself in the appearance of new bands at 2127, 2054, 2017, and 1949 cm<sup>-1</sup> due to crystalline TA (Figure 1b, purple trace). These bands can also be observed in the control experiment (Figure S2 in the Supplementary Materials) and this finding is in complete agreement with the results of earlier studies with TA ices [14]. Then, TA starts subliming, which is also reflected in the difference spectra taken at 250 K; the ACN band is already disappeared by this temperature (Figure 1b, dark yellow trace). Lastly, no sample remains on the substrate at temperature of 300 K (Figure 1b, turquoise trace). The behavior of the third product ([CN]<sup>-</sup>) is more dubious but its production seems increasing with temperature, a detailed analysis is given in Section 4.3.

### 3.2. Electron Bombardment of TA:H<sub>2</sub>O Ice Mixture

In order to assess the effect of H<sub>2</sub>O ice, a common constituent of interstellar ices and an O atom source, the experiment was repeated, mixed with H<sub>2</sub>O (Figure 2a, black trace). The band maxima of the precursor suffer some shift when mixed with H<sub>2</sub>O as listed in Table S5 in the Supplementary Materials. When exposed to high-energy electrons, the bands belonging to the precursors evidently decrease, whereas new bands appear according to the formation of irradiation products. Most of them have similar band profile and position, therefore can be attributed to the same species that form during the irradiation of pure amorphous TA. The maxima of these bands lie at 2290, 2259, 2083, and 2037 cm<sup>-1</sup> (Figure 2a, red trace); they can be assigned to ACN, [CN]<sup>-</sup>, and H<sub>2</sub>C=C=NH, respectively (Table 2). One new band that can be observed in the TA:H<sub>2</sub>O ice mixture upon electron bombardment is a broad feature at 2168 cm<sup>-1</sup>, which is probably due to the isocyanate anion ([OCN]<sup>-</sup>). This species was found in earlier irradiation studies involving ACN:H<sub>2</sub>O mixtures [27].

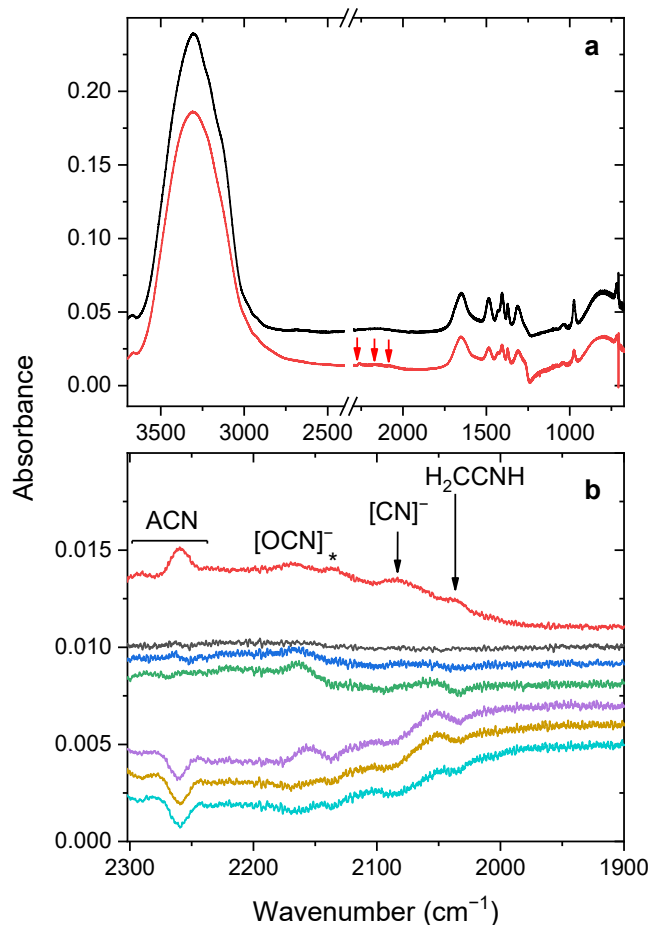


**Figure 2.** (a) MIR spectra (3600–675 cm<sup>-1</sup> region) of the TA:H<sub>2</sub>O ice mixture in the control (black trace) and electron bombardment (red trace) experiments. The red arrows show the newly forming bands. (b) MIR spectra (2300–1900 cm<sup>-1</sup> region) of the TA:H<sub>2</sub>O ice mixture in the beginning of the TPD phase (red trace). Difference spectra as obtained at 50 K (dark gray), 100 K (blue), 150 K (green), 200 K (purple), 250 K (dark yellow), and 300 K (turquoise), respectively; the spectra taken at the beginning of the TPD phase served as reference. The spectra are offset for clarity. The band at ≈ 2136 cm<sup>-1</sup> marked with an asterisk is probably due to CO from the radiolysis of CO<sub>2</sub> impurity.

Figure 2b shows the spectrum right at the start of the TPD process (black trace) as well as the changes when the sample was warmed up (see full spectra in Figure S3 in the Supplementary Materials). Accordingly, the H<sub>2</sub>C=C=NH band at 2037 cm<sup>-1</sup> already starts to diminish at 100 K (blue trace) and is completely gone by 150 K (green trace). In contrast, the ACN bands are still visible at 150 K and only disappear by 200 K (purple trace). The fate of the [OCN]<sup>-</sup> band is less straightforward but, based on the difference spectra, seems to somewhat increase in the temperature range of 100–200 K and only disappears by 250 K (dark yellow trace). The qualitative behavior of the [CN]<sup>-</sup> band is even more ambiguous. The spectra of the control experiment does not exhibit any similar changes during TPD (Figure S4 in the Supplementary Materials).

**Table 2.** Assignment of the bands appearing during electron irradiation of TA:H<sub>2</sub>O ice mixture.

Wavenumber (cm <sup>-1</sup> )	Literature Value	Molecule	Assignment <sup>a</sup>	Ref.
2290	2289	ACN	$\nu[\text{CC}] + \beta_s[\text{CH}_3]$ <sup>b</sup>	[25]
2259	2252	ACN	$\nu[\text{C}\equiv\text{N}]$	[25]
2168	2166	[OCN] <sup>-</sup>	$\nu[[\text{OCN}]^-]$	[27]
2083	2081	[CN] <sup>-</sup>	$\nu[[\text{CN}]^-]$	[27,28]
2037	2033	H <sub>2</sub> C=C=NH	$\nu_{\text{as}}[\text{C}=\text{C}=\text{NH}]$	[27]

<sup>a</sup>  $\nu$ : stretching;  $\beta$ : bending; s: symmetric; as: antisymmetric; <sup>b</sup> Combination band. Assignment made based on anharmonic computations at the B3LYP/cc-pVTZ level of theory using the Gaussian G09 software [19]; Fermi-resonance is predicted with the  $\nu[\text{C}\equiv\text{N}]$  mode.

## 4. Discussion

### 4.1. Irradiation of Neat TA Ices and TA:H<sub>2</sub>O Ice Mixtures

In order to quantitatively assess the changes occurring in the samples during their exposure to energetic electrons, kinetic curves have to be produced. This is done by calculating  $N$  (Section 2) of each detected species and plotting them against dose. The  $N$  values can be obtained by using the following modified Lambert-Beer equation [2]:

$$N = \frac{\ln 10 \int A(\tilde{\nu}) d\tilde{\nu} \cos \alpha}{A'_i \cdot 2}$$

where  $A(\tilde{\nu})$  designates the experimental intensity at wavenumber  $\tilde{\nu}$  (in cm<sup>-1</sup>), and  $A'_i$  indicates the absolute band strength of vibrational mode  $i$  (in cm molecule<sup>-1</sup>).  $\alpha$  signifies the angle between the surface normal of the IR beam and the substrate (60° in vacuum), dividing it by two corrects for the incoming and outgoing IR beams. It is worth noting, however, that the refractive index  $n$  of TA and H<sub>2</sub>O differs from unity, thus,  $\alpha$  is different in the ice than in vacuum. This can be calculated using Snell's law, taking into account  $n = 1.522$  of crystalline TA as predicted by the Advanced Chemistry Development (ACD/Labs) Software (Toronto, ON, Canada) (changing  $\alpha$  to 35°). The used average value of  $n$  for the TA:H<sub>2</sub>O mixture was 1.35 by taking  $n = 1.32$  of crystalline water ice (changing  $\alpha$  to 43°) [33].

It should also be noted that the experimental  $A'_i$  values are not known for TA, thus, they had to be estimated computationally. For this, the same (dodecamer) crystalline model were used as in Góbi et al. (2020) [14]; to simulate the spectra, the theoretical harmonic vibrational frequencies (scaling factor: 0.975) and computed IR intensities (not scaled) were convoluted with Lorentzian functions with an FWHM of 4 cm<sup>-1</sup>. The obtained fitting curves were then integrated for each band belonging to a specific vibrational mode thus estimating the  $A'_i$  values (summarized in Table 3) used to calculate the  $N$  values, which latter were averaged and their standard deviation was also calculated. The  $N$  values of the irradiation products were calculated similarly, using the 2252 cm<sup>-1</sup> band of ACN ( $A' = 2.2 \times 10^{-18}$  cm molecule<sup>-1</sup>) as well as the 2029 cm<sup>-1</sup> one of H<sub>2</sub>C=C=NH ( $7.2 \times 10^{-17}$  cm molecule<sup>-1</sup>) [27], and that of [CN]<sup>-</sup> at 2068 cm<sup>-1</sup> ( $6.9 \times 10^{-18}$  cm molecule<sup>-1</sup>) [34]. Figure 3a visualizes the change in  $N$  of the precursor as well as the those of the products during electron bombardment (the full version of the graph can be seen in Figure S5 in the Supplementary Materials).

It can be seen that as  $N$  of the TA precursor monotonically decreases during the sample exposure to the high-energy electrons, those of the decomposition products increase throughout the electron bombardment. The calculated  $N$  values of ACN and [CN]<sup>-</sup> are similar, however, those of the third product (H<sub>2</sub>C=C=NH) are more than an order of magnitude lower than that of its isomeric counterpart. It is known that ACN undergoes isomerization when exposed to UV or p<sup>+</sup> irradiation [27]. Thus, this finding may be explained by the fact that H<sub>2</sub>C=C=NH is a secondary product, i.e., it forms from ACN via its electron-induced isomerization. An alternative explanation would be a less efficient direct formation from the TA precursor. For this, one should bear in mind that the formation of both ACN and H<sub>2</sub>C=C=NH from TA requires the formal elimination of H<sub>2</sub>S. Even though no evidence could be found for the existence of the latter in the processed sample, its formation and thus the direct formation of H<sub>2</sub>C=C=NH from the precursor cannot be ruled out as the absorption bands of H<sub>2</sub>S are typically weak in the ice phase [35]. This kinetics shows some resemblance with that obtained in inert matrices upon UV irradiation, with some evident differences [15]. One of them is the lack of thiols, which are actually the first species appearing in the exposed sample in matrix-isolated environments. Furthermore, H<sub>2</sub>C=C=NH behaves as a primary product and its formation precedes that of its isomer, ACN. Nevertheless, the mixing ratio of the former is significantly lower than the latter in cryogenic matrices, similarly to what is observed in amorphous ices. Finally, the kinetics of ACN is more different in matrices than in amorphous ices [15], whereas HCN seemingly starts to

form at a later stage of the irradiation in a cryogenic matrix than  $[\text{CN}]^-$  in the current study. One should also emphasize that the current study used electron irradiation, whereas the matrix-isolated samples were UV irradiated. It was, however, difficult to deduce sound conclusions based on the changes in  $N$  in matrices, and the same applies to the amorphous ice phase here.

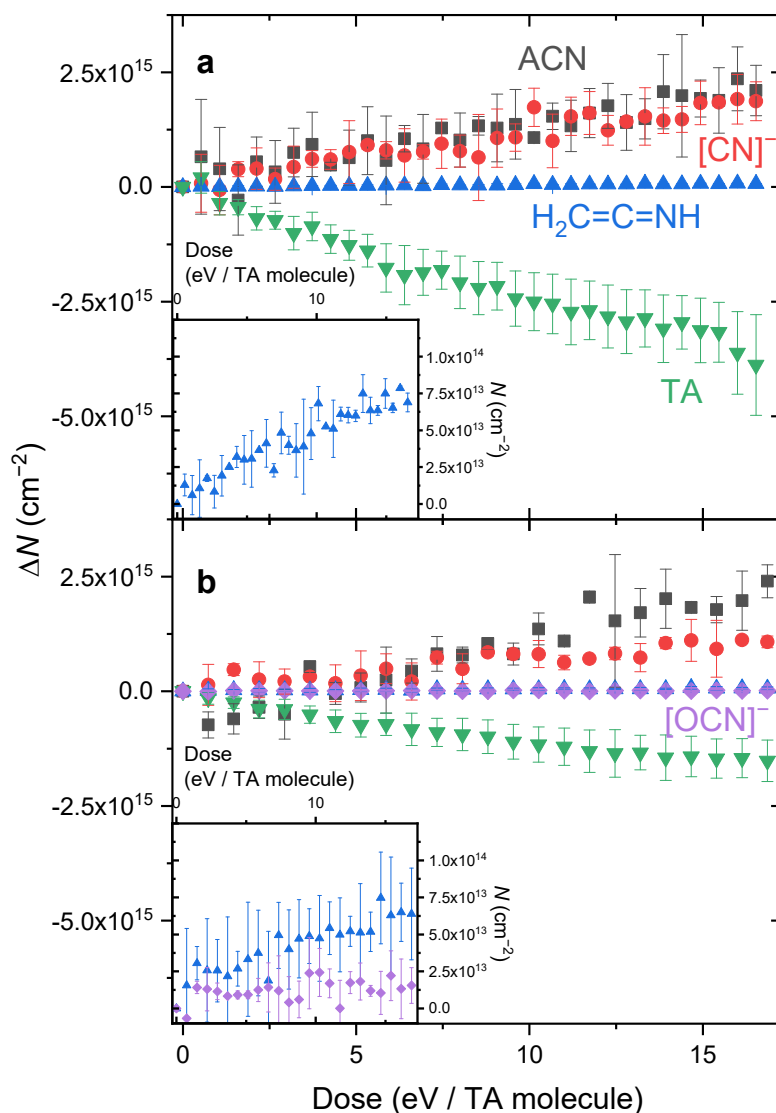


**Figure 3.** Change of  $N$  of TA (green upside-down triangles) as well as the products ACN (black squares),  $[\text{CN}]^-$  (red circles), and  $\text{H}_2\text{C}=\text{C}=\text{NH}$  (blue triangles) during the fourth electron bombardment cycle of (a) the neat amorphous TA experiment; (b) the TA: $\text{H}_2\text{O}$  experiment. The insets show blowups of the figures for  $\text{H}_2\text{C}=\text{C}=\text{NH}$  and  $[\text{OCN}]^-$ .

**Table 3.** Estimated  $A'_i$  values of the bands used to determine  $N$  of the neat TA ice.

Integration Boundaries ( $\text{cm}^{-1}$ )	$A'_i$ (in cm)	Assignment <sup>a</sup>
1713–1608	$4.0 \pm 10^{-17}$	$\beta[\text{NH}_2]$
1535–1459	$3.5 \pm 10^{-17}$	$(-)\nu[\text{CN}]$ & $\beta_{\text{as}}$ , i.p.[ $\text{CH}_3$ ]
1457–1379	$5.0 \pm 10^{-17}$	$\beta_{\text{as}}$ , o.p.[ $\text{CH}_3$ ], $(+)\nu[\text{CN}]$ & $\beta_{\text{as}}$ , i.p.[ $\text{CH}_3$ ]
1383–1354	$1.2 \pm 10^{-17}$	$\beta_{\text{s}}[\text{CH}_3]$
1337–1279	$1.7 \pm 10^{-17}$	$\rho[\text{NH}_2]$
1005–956	$1.8 \pm 10^{-17}$	$\nu[\text{CC}]$

<sup>a</sup> Assignment based on Góbi et al. (2020) [14].  $\nu$ : stretching;  $\beta$ : bending;  $\rho$ : rocking;  $s$ : symmetric;  $as$ : antisymmetric;  $i.p.$ : in-plane;  $o.p.$ : out-of-plane vibrations; &: resonance between the listed vibrational modes. The signs  $(-)$  and  $(+)$  denote in-phase and opposite-phase couplings between the coordinates that participate in the resonance.

By having a look at Figure 3b, one can see that the presence of H<sub>2</sub>O does not change the overall kinetics remarkably. In general, the  $N$  values of both the products and the precursor are similar to that obtained in the pure TA ice. However, the formation of [CN]<sup>-</sup> might become less efficient probably because of its conversion further into [OCN]<sup>-</sup>, whereas the consumption rate of TA appears to be lower. This apparent difference from the pure TA sample may be due to the fact that the same absorption coefficients were used for the sample containing H<sub>2</sub>O, which may significantly alter the environment of the TA molecules. Besides, the formation of [OCN]<sup>-</sup>, which—based on its column density—is a minor product, since it is produced in an amount even lower than H<sub>2</sub>C=C=NH. The  $N$  value of [OCN]<sup>-</sup> was determined using its 2168 cm<sup>-1</sup> band ( $A' = 1.3 \times 10^{-16}$  cm molecule<sup>-1</sup>) [36].

#### 4.2. Elemental Balances during Electron Bombardment

Interesting conclusions can be drawn when the amount of elements occurring in the decomposition products is compared to those in the decayed TA precursor (Table 4). The table lists the C and N balances, and makes an attempt to estimate that of S, even though no carriers of the S atom (such as H<sub>2</sub>S) could be identified in the processed sample, most likely due to their extremely weak absorption bands. The formation of refractory residue on the substrate surface (such as elemental sulfur) is another possible explanation for the apparent lack of sulfur carriers.

**Table 4.** Changes in the amount of the precursor as well as the decomposition products in the TA and TA:H<sub>2</sub>O samples after the samples absorbed the same dose of 16 eV/TA molecule <sup>a</sup>.

Species	$\Delta N$ (cm <sup>-2</sup> )	
	Neat TA	TA:H <sub>2</sub> O
TA	$-(3.9 \pm 1.1) \times 10^{15}$	$-(1.5 \pm 0.4) \times 10^{15}$
ACN	$(2.1 \pm 0.6) \times 10^{15}$	$(2.0 \pm 0.7) \times 10^{15}$
[CN] <sup>-</sup>	$(1.9 \pm 0.4) \times 10^{15}$	$(1.1 \pm 0.1) \times 10^{15}$
H <sub>2</sub> C=C=NH	$(6.9 \pm 0.6) \times 10^{13}$	$(6.5 \pm 2.0) \times 10^{13}$
[OCN] <sup>-</sup>	—	$(1.3 \pm 2.0) \times 10^{13}$
H <sub>2</sub> S	$1 \times 10^{14}$	$1 \times 10^{14}$
C balance	80 ± 33%	175 ± 65%
N balance	104 ± 57%	212 ± 112%
S balance	<3%	<7%

<sup>a</sup> When calculating elemental balances, it has to be taken into consideration that the TA, ACN, and H<sub>2</sub>C=C=NH molecules contain two C atoms. In the case of H<sub>2</sub>S, an upper estimate could be provided.

No significant differences can be observed in the amount of the irradiation products except [CN]<sup>-</sup>, which are present in both samples (i.e., ACN and H<sub>2</sub>C=C=NH). The amount of [OCN]<sup>-</sup> is so low that it does not significantly influence the overall elemental balances. Still, the apparent elemental balances of the two experiments differ by a factor of two, which can be explained by the calculated lower  $N$  value of the destroyed TA molecules in the sample also containing H<sub>2</sub>O. It should be noted that, owing to the lack of data, the absorption coefficients estimated for the neat TA ice were used for the TA:H<sub>2</sub>O samples as well. This assumption does not take into account the fact that the absorption coefficients in ice phase are sensitive to the environment and the presence of H<sub>2</sub>O may significantly change those of the TA molecules. The C and N balances nearly double to 170–210% in the processed H<sub>2</sub>O-containing ice with regard to the neat TA sample, which suggest the underestimation of TA column density in the presence of H<sub>2</sub>O molecules. And indeed, the  $N$  value of TA in the TA–H<sub>2</sub>O sample is estimated to be around half as much as in the pure TA sample (Table 4). This may be caused by the significant change in the absorption coefficients of the TA molecule when surrounded by H<sub>2</sub>O molecules. Alternatively, the  $N$  values of the products may be overestimated, although they are in accordance with those obtained in the pure TA ice, in contrast to what could be found for the precursor molecule.

Even so, the C and N atoms in the products account for approximately 100% of those of the decomposed TA molecules in the neat sample, which, interestingly, is significantly higher than those observed in cryogenic matrices, when exposed to H atoms (≈10%) or UV irradiation (≈30%) [15,16]. This discrepancy may be explained by taking into account that the absorption coefficients of the amorphous ice sample are less reliable than those obtained for cryogenic matrices, which may make the difference an apparent one only. One should also address the ≈40–50% relative uncertainty of the obtained elemental balances. The final balance is obtained by dividing the number of either C or N atoms in the product (e.g., in ACN) by that of the TA molecule. These numbers are proportional to the  $N$  values, whose relative uncertainty is ≈30%. The division results in even higher uncertainties due to error propagation.

One may also provide an upper estimate of H<sub>2</sub>S by taking into account the detection limit of the spectrometer and the absorption coefficient of the molecule as obtained by Jiménez-Escobar et al. (2011) [ $2 \times 10^{-17}$  cm/molecule] [35]. As we found for our system, integrated band areas smaller than 0.002 absorbance unit cannot be distinguished from background noise, thus it can be deduced that the column density for H<sub>2</sub>S cannot be higher than  $1 \times 10^{-14}$  cm<sup>2</sup> varying slightly depending on whether the sample contains H<sub>2</sub>O or not. This also enables to estimate the S balance as well (Table 4). As it can be seen, this estimated amount accounts for only several percent of all sulfur atoms released by the destruction of the precursor molecules. This points to the possibility of formation of other sulfurous compounds, such as elemental sulfur, that may go undetected due to their IR inactivity.

#### 4.3. Processed Neat TA Ices and TA:H<sub>2</sub>O Ice Mixtures during TPD

The changes of  $N$  can also be obtained during the TPD phase of the experiment. Figure 4a shows those of the electron irradiation products allowing the more accurate determination of sublimation temperatures. As one may notice,  $N$  of ACN stays constant until the temperature of ca. 180 K, after which it steadily diminishes and reaches zero by 255 K. The sublimation temperature of pure ACN was found to be much lower, around 155 K or 125–145 K depending on the study [27,28]; the discrepancy may be explained by the entrapment of ACN in the less volatile TA ice structure. The amount of [CN]<sup>-</sup> stays constant until approximately 170 K when it gradually becomes zero by room temperature. Unfortunately, previous works did not specify the TPD curve of [CN]<sup>-</sup>, only that of its protonated counterpart (HCN), disclosing a sublimation event at around 120 K [28]. The minor product, H<sub>2</sub>C=C=NH, has a TPD profile completely different than that of the two aforementioned compounds; it is stable up to the temperature of 100 K, from which point it steadily decreases and the signal is entirely absent by 140 K. The desorption temperature of H<sub>2</sub>C=C=NH shares similarities with the values presented in earlier works (85 K) [28].

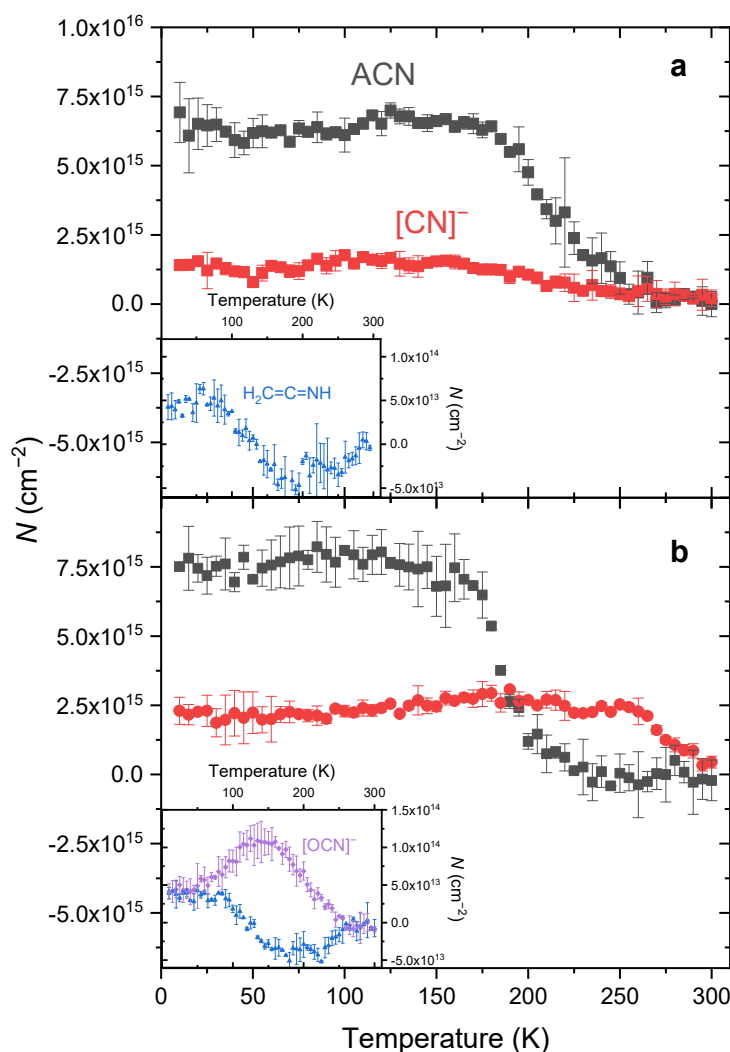


**Figure 4.** (a)  $N$  of ACN (black squares), [CN]<sup>-</sup> (red circles), and H<sub>2</sub>C=C=NH (inset, blue triangles) during TPD of the electron bombarded neat TA sample. (b)  $N$  of ACN (black squares), [OCN]<sup>-</sup> (inset, purple rectangles), [CN]<sup>-</sup> (red circles), and H<sub>2</sub>C=C=NH (inset, blue triangles) during TPD of the electron bombarded TA-H<sub>2</sub>O sample.

One can observe some similarities when looking at the TPD curves of the electron-irradiated TA:H<sub>2</sub>O ices (Figure 4b). For instance, ACN start to sublime at 180 K, whereas the sublimation event of H<sub>2</sub>C=C=NH starts at 95 K. Both values are close to the ones obtained in the processed neat TA ice. In contrast, the mixing ratio of [CN]<sup>-</sup> appears to be constant up until 260 K, which contradicts the results of the neat TA ice experiment. The fourth product, [OCN]<sup>-</sup>, should also be mentioned, it shows a maximum at around 140 K, from which point it gradually diminishes. According to Hudson & Moore [27], in irradiated ACN:H<sub>2</sub>O ice mixtures, H<sub>2</sub>C=C=NH was still present in the sample at 125 K, with some residues at 150 K. Furthermore, they still observed the [OCN]<sup>-</sup> ion at temperatures as high as 200 K. These findings are in line with the results of our experiment.

## 5. Conclusions

When amorphous TA ices are exposed to high-energy electrons, they decompose into the C<sub>2</sub>H<sub>2</sub>N isomers ACN and H<sub>2</sub>C=C=NH, possibly through H<sub>2</sub>S elimination. However, there is no experimental proof for the presence of the latter, likely due to the weak IR absorption of solid-phase H<sub>2</sub>S. Alternatively, the formation of nascent sulfur or small sulfur clusters could be another plausible explanation. The formation of [CN]<sup>-</sup> can be also proven. The presence of H<sub>2</sub>O, acting as an O source, alters the decomposition mechanism so that the exposed TA:H<sub>2</sub>O ices also contain [OCN]<sup>-</sup>. The assignment was corroborated based on the decay kinetics and the band changes during TPD. Furthermore, some conclusions can be deduced with regards to the decomposition mechanism. According to these, ACN and [CN]<sup>-</sup> are primary products, whereas H<sub>2</sub>C=C=NH and [OCN]<sup>-</sup> are minor ones. These findings are comparable to ones obtained when TA dispersed in cryogenic matrices was exposed to energetic radiation. In contrast, the decomposition appears to be more efficient in the amorphous ice phase than in matrix-isolated environment [15], based on the elemental balances, even though this apparent difference may also be explained by the assumptions made to estimate the absorption coefficients of the amorphous samples. The results presented here may also be interesting in the context of astrochemistry, like sulfur depletion. Even though TA has not been explicitly detected in space, it has been searched for and upper limits to its *N* were provided [37,38]. Besides, the related molecule thioacetaldehyde (H<sub>3</sub>C-C(=S)H) has just been detected in the interstellar medium pointing to the potential relevance of thiones in space [39]. Furthermore, H<sub>2</sub>O is an important interstellar ice constituent; thus, its influence on the decay mechanism of sulfurous molecules is a relevant issue.

## Supplementary Materials

The additional data and information can be downloaded at: <https://media.scilitp.com/articles/others/2511191503331129/PS-25100008-SM-FC-done.pdf>. Table S1: Cartesian coordinates (Å) of ACN as optimized at the B3LYP/cc-pVTZ level of theory. Table S2: Harmonic and anharmonic IR vibrational frequencies and intensities of ACN as computed at the B3LYP/cc-pVTZ level of theory. Table S3: Summary of the CASINO simulations performed on the electron bombardment experiments. Table S4: Infrared bands of neat amorphous TA ice. Table S5: Infrared bands of the amorphous TA–H<sub>2</sub>O ice mixture. Figure S1: MIR spectra (3600–675 cm<sup>-1</sup> region) of processed TA ice in the beginning of the TPD phase (black trace), at 50 K (red), 100 K (blue), 150 K (green), 200 K (purple), 250 K (dark yellow), and 300 K (turquoise), respectively. The spectra are offset for clarity. Figure S2: MIR spectra (3600–675 cm<sup>-1</sup> region) of neat TA ice (blank experiment) in the beginning of the TPD phase (black trace), at 50 K (red), 100 K (blue), 150 K (green), 200 K (purple), 250 K (dark yellow), and 300 K (turquoise), respectively. The spectra are offset for clarity. Figure S3: MIR spectra (3600–675 cm<sup>-1</sup> region) of processed TA–H<sub>2</sub>O ice mixture in the beginning of the TPD phase (black trace), at 50 K (red), 100 K (blue), 150 K (green), 200 K (purple), 250 K (dark yellow), and 300 K (turquoise), respectively. The spectra are offset for clarity. Figure S4: MIR spectra (3600–675 cm<sup>-1</sup> region) of the neat TA–H<sub>2</sub>O ice mixture (blank experiment) in the beginning of the TPD phase (black trace), at 50 K (red), 100 K (blue), 150 K (green), 200 K (purple), 250 K (dark yellow), and 300 K (turquoise), respectively. The spectra are offset for clarity. Figure S5: Change of *N* of TA (green upside-down triangles) as well as the products ACN (black squares), [CN]<sup>-</sup> (red circles), and H<sub>2</sub>C=C=NH (blue triangles) during the fourth electron bombardment cycle of (a) the neat amorphous TA experiment; (b) the TA–H<sub>2</sub>O experiment (full version). The insets show blowups of the figures for H<sub>2</sub>C=C=NH and [OCN]<sup>-</sup>.

## Author Contributions

S.G.: Conceptualization, Data curation, Formal analysis, Funding Acquisition, Investigation, Methodology, Project administration, Supervision, Validation, Visualization, Writing—original draft, Writing—review & editing. B.K.: Investigation, Writing—review & editing. G.T.: Funding acquisition, Project administration, Resources, Supervision, Writing—review & editing. All authors have read and agreed to the published version of the manuscript.

## Funding

The authors thank the Hungarian Scientific Research Fund (No. OTKA K143196) and the Thematic Excellence Program of the Eötvös Loránd University (No. TKP2021-NKTA-64), both from the fund of the National Research, Development and Innovation Office (NKFIH). S.G. was supported by the “Bolyai” scholarship of the Hungarian Academy of Sciences (MTA). B.K. acknowledges the “DKÖP-23 Doctoral Excellence Program” of the Ministry for Culture and Innovation (KIM) from the source of NKFIH.

## Institutional Review Board Statement

Not applicable.

## Informed Consent Statement

Not applicable.

## Data Availability Statement

The data underlying this article are available in the article and in its supplementary material. Additional data that support the findings of this study are available from the corresponding author upon request.

## Conflicts of Interest

Given the role as Editorial Board Member, Sándor Góbi had no involvement in the peer review of this paper and had no access to information regarding its peer-review process. Full responsibility for the editorial process of this paper was delegated to another editor of the journal.

## Use of AI and AI-Assisted Technologies

No AI tools were utilized for this paper.

## References

1. Mifsud, D.V.; Kaňuchová, Z.; Herczku, P.; et al. Sulfur Ice Astrochemistry: A Review of Laboratory Studies. *Space Sci. Rev.* **2021**, *217*, 14. <https://doi.org/10.1007/s11214-021-00792-0>.
2. Bennett, C.J.; Jamieson, C.; Mebel, A.M.; et al. Untangling the Formation of the Cyclic Carbon Trioxide Isomer in Low Temperature Carbon Dioxide Ices. *Phys. Chem. Chem. Phys.* **2004**, *6*, 735–746. <https://doi.org/10.1039/b315626p>.
3. Wu, Q.T.; Anderson, H.; Watkins, A.K.; et al. Role of Low-Energy (<20 eV) Secondary Electrons in the Extraterrestrial Synthesis of Prebiotic Molecules. *ACS Earth Space Chem.* **2024**, *8*, 79–88. <https://doi.org/10.1021/acsearthspacechem.3c00259>.
4. Carlson, R.W.; Anderson, M.S.; Johnson, R.E.; et al. Sulfuric Acid Production on Europa: The Radiolysis of Sulfur in Water Ice. *Icarus* **2002**, *157*, 456–463. <https://doi.org/10.1006/icar.2002.6858>.
5. Maity, S.; Kim, Y.S.; Kaiser, R.I.; et al. On the Detection of Higher Order Carbon Sulfides (CS<sub>x</sub>; X = 4–6) in Low Temperature Carbon Disulfide Ices. *Chem. Phys. Lett.* **2013**, *577*, 42–47. <https://doi.org/10.1016/j.cplett.2013.05.039>.
6. Maity, S.; Kaiser, R.I. Electron Irradiation of Carbon Disulfide-Oxygen Ices: Toward the Formation of Sulfur-Bearing Molecules in Interstellar Ices. *Astrophys. J.* **2013**, *773*, 184. <https://doi.org/10.1088/0004-637X/773/2/184>.
7. Sivaraman, B. Electron Irradiation of Carbon Dioxide-Carbon Disulphide Ice Analog and Its Implication on the Identification of Carbon Disulphide on Moon. *J. Chem. Sci.* **2016**, *128*, 159–164. <https://doi.org/10.1007/s12039-015-0996-6>.
8. Mahjoub, A.; Poston, M.J.; Blacksberg, J.; et al. Production of Sulfur Allotropes in Electron Irradiated Jupiter Trojans Ice Analogs. *Astrophys. J.* **2017**, *846*, 148. <https://doi.org/10.3847/1538-4357/aa85e0>.
9. Mifsud, D.V.; Herczku, P.; Rácz, R.; et al. Energetic Electron Irradiations of Amorphous and Crystalline Sulphur-Bearing Astrochemical Ices. *Front. Chem.* **2022**, *10*, 1003163. <https://doi.org/10.3389/fchem.2022.1003163>.
10. Wang, J.; Marks, J.H.; Tuli, L.B.; et al. Formation of Thioformic Acid (HCOSH)—The Simplest Thioacid—in Interstellar Ice Analogues. *J. Phys. Chem. A* **2022**, *126*, 9699–9708. <https://doi.org/10.1021/acs.jpca.2c06860>.
11. Martín-Doménech, R.; Öberg, K.I.; Muñoz Caro, G.M.; et al. Ice Origins of OCS and Chemistry of CS<sub>2</sub>-Bearing Ice Mantles. *Mon. Not. R. Astron. Soc.* **2024**, *535*, 807–825. <https://doi.org/10.1093/mnras/stae2345>.
12. Góbi, S.; Keresztes, B.; Schneiker, A.; et al. UV Photolysis of Thiourea and Its *N*-Methylated Derivative in Cryogenic Matrices. *Phys. Chem. Chem. Phys.* **2024**, *26*, 9963–9974. <https://doi.org/10.1039/d4cp00016a>.
13. Góbi, S.; Keresztes, B.; Schneiker, A.; et al. Hydrogen-Atom-Assisted Thione–Thiol Tautomerization of Thiourea Derivatives in *para*-H<sub>2</sub> Matrix. *J. Chem. Phys.* **2025**, *162*, 174306. <https://doi.org/10.1063/5.0265542>.
14. Góbi, S.; Reva, I.; Tarczay, G.; et al. Amorphous and Crystalline Thioacetamide Ice: Infrared Spectra as a Probe for

- Temperature and Structure. *J. Mol. Struct.* **2020**, *1220*, 128719. <https://doi.org/10.1016/j.molstruc.2020.128719>.
15. Góbi, S.; Keresztes, B.; Schneiker, A.; et al. Energetic Processing of Thioacetamide in Cryogenic Matrices. *J. Chem. Phys.* **2024**, *160*, 024310. <https://doi.org/10.1063/5.0177587>.
  16. Góbi, S.; Keresztes, B.; Schneiker, A.; et al. Hydrogen-Atom-Assisted Processes on Thioacetamide in *para*-H<sub>2</sub> Matrix—Formation of Thiol Tautomers. *Phys. Chem. Chem. Phys.* **2024**, *26*, 21589–21597. <https://doi.org/10.1039/d4cp02400a>.
  17. Góbi, S.; Reva, I.; Ragupathy, G.; et al. Hydrogen-Atom-Assisted Tautomerization on Solid Surfaces—The Case Study of Thioacetamide. *J. Phys. Chem. C* **2024**, *128*, 21691–21701. <https://doi.org/10.1021/acs.jpcc.4c05817>.
  18. Bazsó, G.; Csonka, I.P.; Góbi, S.; et al. VIZSLA—Versatile Ice Zigzag Sublimation Setup for Laboratory Astrochemistry. *Rev. Sci. Instrum.* **2021**, *92*, 124104. <https://doi.org/10.1063/5.0061762>.
  19. Frisch, M.J.; Trucks, G.W.; Schlegel, H.B.; et al. *Gaussian 09, Revision D.01*; Gaussian, Inc.: Wallingford, CT, USA, 2009.
  20. Barone, V. Anharmonic Vibrational Properties by a Fully Automated Second-Order Perturbative Approach. *J. Chem. Phys.* **2005**, *122*, 014108. <https://doi.org/10.1063/1.1824881>.
  21. Bloino, J.; Barone, V. A Second-Order Perturbation Theory Route to Vibrational Averages and Transition Properties of Molecules: General Formulation and Application to Infrared and Vibrational Circular Dichroism Spectroscopies. *J. Chem. Phys.* **2012**, *136*, 124108. <https://doi.org/10.1063/1.3695210>.
  22. Hambley, T.W.; Hibbs, D.E.; Turner, P.; et al. Insights into Bonding and Hydrogen Bond Directionality in Thioacetamide from the Experimental Charge Distribution. *J. Chem. Soc. Perkin Trans.* **2002**, *2*, 235–239. <https://doi.org/10.1039/b109353c>.
  23. Schmitt, B.; de Bergh, C.; Festou, M. Solar System Ices. In *Astrophysics and Space Science Library*; Schmitt, B., De Bergh, C., Festou, M., Eds.; Springer: Dordrecht, The Netherlands, 1998; Volume 227, ISBN 978-94-010-6209-1.
  24. Drouin, D.; Couture, A.R.; Joly, D.; et al. CASINO V2.42—A Fast and Easy-to-use Modeling Tool for Scanning Electron Microscopy and Microanalysis Users. *Scanning* **2007**, *29*, 92–101. <https://doi.org/10.1002/sca.20000>.
  25. Rachid, M.G.; Rocha, W.R.M.; Linnartz, H. Infrared Spectra of Complex Organic Molecules in Astronomically Relevant Ice Mixtures V. Methyl Cyanide (Acetonitrile). *Astron. Astrophys.* **2022**, *665*, A89. <https://doi.org/10.1051/0004-6361/202243417>.
  26. Hager, T.J.; Moore, B.M.; Borengasser, Q.D.; et al. VUV Processing of Nitrile Ice: Direct Comparison of Branching in Ice and TPD Spectra. *ACS Earth Space Chem.* **2025**, *9*, 2137–2147. <https://doi.org/10.1021/acsearthspacechem.5c00133>.
  27. Hudson, R.L.; Moore, M.H. Reactions of Nitriles in Ices Relevant to Titan, Comets, and the Interstellar Medium: Formation of Cyanate Ion, Ketenimines, and Isonitriles. *Icarus* **2004**, *172*, 466–478. <https://doi.org/10.1016/j.icarus.2004.06.011>.
  28. Chuang, K.J.; Jäger, C.; Santos, J.C.; et al. Formation of N-Bearing Complex Organic Molecules in Molecular Clouds: Ketenimine, Acetonitrile, Acetalimine, and Vinylamine via the UV Photolysis of C<sub>2</sub>H<sub>2</sub> Ice. *Astron. Astrophys.* **2024**, *687*, A7. <https://doi.org/10.1051/0004-6361/202348890>.
  29. Polak, M.; Gruebele, M.; Saykally, R.J. Velocity Modulation Diode Laser Spectroscopy of Negative Ions: The  $\nu_1$ ,  $\nu_1+\nu_2-\nu_2$ ,  $\nu_1+\nu_3-\nu_3$  Bands of Thiocyanate (NCS<sup>-</sup>). *J. Chem. Phys.* **1987**, *87*, 3352–3356. <https://doi.org/10.1063/1.453030>.
  30. Herrero, V.J.; Tanarro, I.; Jiménez-Serra, I.; et al. Stability of Urea in Astrophysical Ices. A Laboratory Study of VUV Irradiation and High-Energy Electron Bombardment. *Mon. Not. R. Astron. Soc.* **2022**, *517*, 1058–1070. <https://doi.org/10.1093/mnras/stac2658>.
  31. Gerakines, P.A.; Moore, M.H.; Hudson, R.L. Ultraviolet Photolysis and Proton Irradiation of Astrophysical Ice Analogs Containing Hydrogen Cyanide. *Icarus* **2004**, *170*, 202–213. <https://doi.org/10.1016/j.icarus.2004.02.005>.
  32. Durig, J.R.; Wertz, D.W. On the Infrared Spectra of HNCS and DNCS. *J. Chem. Phys.* **1967**, *46*, 3069–3077. <https://doi.org/10.1063/1.1841178>.
  33. Mastrapa, R.M.; Bernstein, M.P.; Sandford, S.A.; et al. Optical Constants of Amorphous and Crystalline H<sub>2</sub>O-Ice in the near Infrared from 1.1 to 2.6  $\mu$ m. *Icarus* **2008**, *197*, 307–320. <https://doi.org/10.1016/j.icarus.2008.04.008>.
  34. Georgieva, M.K.; Velcheva, E.A. Computational and Experimental Studies on the IR Spectra and Structure of the Simplest Nitriles (C<sub>1</sub> and C<sub>2</sub>), Their Anions, and Radicals. *Int. J. Quantum Chem.* **2006**, *106*, 1316–1322. <https://doi.org/10.1002/qua.20887>.
  35. Jiménez-Escobar, A.; Muñoz Caro, G.M. Sulfur Depletion in Dense Clouds and Circumstellar Regions: I. H<sub>2</sub>S Ice Abundance and UV-Photochemical Reactions in the H<sub>2</sub>O-Matrix. *Astron. Astrophys.* **2011**, *536*, A91. <https://doi.org/10.1051/0004-6361/201014821>.
  36. Van Broekhuizen, F.A.; Keane, J.V.; Schutte, W.A. A Quantitative Analysis of OCN<sup>-</sup> Formation in Interstellar Ice Analogs. *Astron. Astrophys.* **2004**, *415*, 425–436. <https://doi.org/10.1051/0004-6361:20034161>.
  37. Maris, A.; Calabrese, C.; Favero, L.B.; et al. Laboratory Measurements and Astronomical Search for Thioacetamide. *ACS Earth Space Chem.* **2019**, *3*, 1537–1549. <https://doi.org/10.1021/acsearthspacechem.9b00084>.
  38. Remijan, A.; Xue, C.; Margulès, L.; et al. Expanding the Submillimeter Wave Spectroscopy and Astronomical Search for Thioacetamide (CH<sub>3</sub>CSNH<sub>2</sub>) in the ISM. *Astron. Astrophys.* **2022**, *658*, A85. <https://doi.org/10.1051/0004-6361/202142504>.
  39. Agúndez, M.; Molpeceres, G.; Cabezas, C.; et al. Detection of Thioacetaldehyde (CH<sub>3</sub>CHS) in TMC-1: Sulfur-Oxygen Differentiation along the Hydrogenation Sequence. *Astron. Astrophys.* **2025**, *693*, L20. <https://doi.org/10.1051/0004-6361/202453459>.